Relativistic nuclear structure effects in $(e,e'\vec{p})$

J. M. Udías and Javier R. Vignote
Departamento de Física Atómica, Molecular y Nuclear, Facultad de Ciencias Físicas,
Universidad Complutense de Madrid, E-28040 Madrid, Spain
(Received 20 July 1999; published 3 August 2000)

Results for recoil nucleon induced polarization for $(e,e'\vec{p})$ are presented using various approximations for the relativistic nucleonic current, at the kinematics of a recent experiment at Bates. We see that the dynamical relativistic effects improve the agreement with the data. We make predictions for the induced normal polarization and responses for TJNAF 89-033 and Mainz A1/2-93 experiments.

PACS number(s): 25.30.Fj, 25.30.Rw, 24.10.−i, 21.60.Cs

I. INTRODUCTION

Several experiments have been proposed or have been carried out to measure the polarization of the ejected nucleon in $(e,e'\vec{p})$ reactions [1–3]. In this way, new sets of polarization response functions can be isolated [4–7].

If we write the cross section for the coincidence $(e,e'\vec{p})$ reaction in terms of recoil nucleon polarization dependent and independent terms, we have [4,6,7]

$$\frac{d^3\sigma_s}{d\epsilon_e d\Omega_e d\Omega'} = \frac{\sigma_0}{2}[1+\vec{P}\cdot\vec{\sigma}], \tag{1}$$

where ϵ_e is the scattered electron energy, σ_0 is the unpolarized cross section, s denotes the nucleon spin projection upon $\vec{\sigma}$, and $\vec{P}$ is the induced polarization. Each of these observables can be written in terms of response functions that are bilinear combinations of the nuclear electromagnetic current operator [4,5,7]. If the electron beam is unpolarized and the experiment is performed in coplanar kinematics $(\phi'=0,\pi)$, the relationship between the nuclear responses and the cross section is given by

$$\frac{d^3\sigma_s}{d\epsilon_e d\Omega_e d\Omega'} = \frac{E'|\vec{P}'|}{2(2\pi^3)}\left[\frac{d\sigma}{d\Omega_e}\right]_{\text{Mott}} \{V_L(R_L+R_L^n\hat{S}_n)+V_T(R_T + R_T^n\hat{S}_n)+\cos\phi' V_{TL}(R_{TL}+R_{TL}^n\hat{S}_n) + \cos 2\phi' V_{TT}(R_{TT}+R_{TT}^n\hat{S}_n)\}. \tag{2}$$

The kinematical factors are $V_L=\lambda^2$, $V_T=\lambda/2+\tan^2\theta_e/2$, $V_{TT}=\lambda/2$, $V_{TL}=\lambda\sqrt{\lambda+\tan^2\theta_e/2}$, and $\lambda=1-(\omega/|\vec{q}|)^2$ where ω and $\vec{q}$ are the energy and momentum transfer in the reaction, θ_e is the electron scattering angle, and E', $|\vec{P}'|$ are the energy and momentum of the ejected nucleon. Hence, for coplanar kinematics, i.e., when the ejected nucleon lies within the electron scattering plane $\vec{P}$, the net ejectile polarization for an unpolarized beam or induced polarization (P_n), is normal to the scattering plane. In the one-photon exchange approximation P_n is zero when no final state interactions (FSI) between the ejected nucleon and the residual system are considered [4,5,7]. Thus, P_n is an observable well suited to study FSI effects in nuclear systems and measurements of P_n at different Q^2 would give information about the onset of nuclear transparency. If nuclear transparency is present at certain Q^2 value, that is, if FSI effects are quenched, we would see a decrease of P_n what would be a clear signature of nuclear transparency free from the ambiguities on the occupancies of the shells under study [9].

The first analysis of the experiment performed at Bates by Woo *et al.* that measured P_n in $^{12}\text{C}(e,e'\vec{p})$ [1] was made in a nonrelativistic framework. Other nonrelativistic results for this experiment were recently presented in Ref. [8]. The nonrelativistic approach to $(e,e'\vec{p})$ is based on the impulse approximation, i.e., assuming the one-photon exchange picture in which the single photon interacts only with the nucleon that is detected [4]. If no FSI are considered, the ejected nucleon is described by a plane wave (plane wave impulse approximation or PWIA). FSI are taken into account using potentials that distort the final nucleon wave function (distorted wave impulse approximation or DWIA) [4]. The nonrelativistic analyses found a a systematic underestimation of P_n of around 10% at best [1].

There are two main sources of an induced nonzero normal polarization in proton knockout reactions caused by the interaction with the residual nucleus in the final state. One is due to the absorption, that is, the flux lost into inelastic channels, parameterized in the imaginary part of the optical potential. Semiclassically, for scattering on a given side of $\vec{q}$, ejecting a nucleon from the front or the rear face of the nucleus would select out different directions of the angular momentum $\vec{l}=\vec{r}\times\vec{p}$ and, as the absorption depends on how much the nucleon travels in the nuclear medium before being detected, the effect is a net induced polarization due to absorption. This is well known from hadronic reactions and is named as the Maris effect or Newns polarization [10]. It is, however, a small source of P_n [1]. The bulk of the induced polarization is primarily due to the real part of the spin-orbit potential, that parametrizes the explicitly spin-dependent terms in the optical potential [1].

Since the spin is a property intrinsically related to relativity, one may *a priori* consider that a relativistic approach is better suited to describe nucleon polarization observables. In recent years, the relativistic mean-field approximation has been successfully used for the analyses of $(e,e'p)$ reactions in the so-called relativistic distorted wave impulse approxi-

mation (RDWIA) [11–15]. The polarization degrees of freedom for the electron and the ejected nucleon have been included in this formalism years ago [7]. In RDWIA, the nucleon current

$$J_N^\mu(\omega,\vec{q})=\int d\vec{p}\,\overline{\psi}_F(\vec{p}+\vec{q})\hat{J}_N^\mu(\omega,\vec{q})\psi_B(\vec{p}) \tag{3}$$

is calculated with relativistic ψ_B and ψ_F wave functions for initial bound and final outgoing nucleons, respectively. $\hat{J}_N^\mu$ is the relativistic nucleon current operator of $cc1$ or $cc2$ forms [16]. As bound state wave function, Dirac-Hartree solutions from relativistic Lagrangian with scalar and vector (SV) meson terms [17] or solutions of Dirac equation with phenomenological Woods-Saxon wells are customarily used. The wave function with asymptotic momentum $\vec{P}'$ for the outgoing proton is a solution of the Dirac equation containing SV optical potentials. Recently a relativistic calculation of P_n following those general lines has appeared [18]. In Ref. [18] it was found that the agreement with the data improved slightly compared to the nonrelativistic analyses of Ref. [1]. However, relativistic effects for this improvement remained unspecified in Ref. [18].

Some of the differences between the relativistic and nonrelativistic approaches are independent of the dynamics, having to do with the proper (relativistic) kinematics being taken into account. Also, the nonrelativistic operators are normally obtained from an expansion and truncation in powers of p/M and sometimes also of q/M and ω/M. When the momenta and energy involved in the reaction are of the order of the nucleon mass, as it may be the case for $(e,e'\vec{p})$ reactions, one must be very careful with the behavior of the expanded and truncated operator. In Ref. [19] different nonrelativistic expansions were studied and new expressions that compared better with the unexpanded result were deduced. In Ref. [8] improved nonrelativistic operators were used, particularly with the inclusion of the extra spin-orbit term in the charge density operator as described in reference [19]. This term proves to be necessary to reproduce at least qualitatively [15,20] the features seen in the R_{TL} response and TL asymmetry

$$A_{TL}=\frac{\sigma(\phi'=\pi)-\sigma(\phi'=0)}{\sigma(\phi'=0)+\sigma(\phi'=\pi)},$$

as measured in a recent TJNAF experiment at $Q^2\simeq 0.8$ $(\mathrm{GeV}/c)^2$ [21].

The nonrelativistic approach can be better compared to the relativistic one thinking in terms of the direct Pauli reduction [13]. Starting from a nonrelativistic formalism based on bispinors χ solutions of a Schrödinger-like equation, one may at best construct properly normalized four-spinors of the form

$$\psi_{\mathrm{NR}}=\frac{1}{\sqrt{N}}\begin{pmatrix}\chi(\vec{p})\\ \dfrac{\vec{\sigma}\cdot\vec{p}}{E+M}\chi(\vec{p})\end{pmatrix} \tag{4}$$

to be introduced in Eq. (3) in order to calculate a relativisticlike nucleon current matrix element. In this way the relativistic kinematics is fully taken into account and no expansions in p/M are needed. One further step to *relativize* the calculations is done by rewriting the Dirac equation for the upper component as a Schrödinger-like equation and introducing its *nonrelativistic* bispinor solution χ in Eq. (4). This ''nonrelativistic'' bispinor is phase shift and energy eigenvalue equivalent to the relativistic solution [13,22,25–27]. Comparing this solution of the Schrödinger-like equation to the upper component of the fully relativistic wave functions, one finds an additional factor (i) so that the upper component of the full Dirac solution is quenched in the nuclear interior compared to the nonrelativistic solution [13,22,25,27]. This quenching can be associated to the Darwin factor [28] that appears from an extra term linear in $\vec{p}$ that must be dealt with to obtain the Schrödinger-like equation and that is not present in the usual nonrelativistic treatment.

One can then build a nonrelativistic formalism based on the Schrödinger-like equation, with central and spin-orbit potentials that are phase shift equivalent to the relativistic potentials, incorporating *a posteriori* the Darwin term in order to recover exactly the same upper component as in RDWIA and, by means of Eq. (4), avoid the expansions in p/M. This formalism would incorporate all the kinematical and operator-related relativistic effects, as well as the dynamical quenching of the relativistic upper components due to the Darwin term.

This is done for instance by Kelly in several works [29] though with an additional approximation, the effective momentum approach (EMA) for the lower components. This amounts to approximate the $\vec{\sigma}\cdot\vec{p}$ term that appears for the lower components in Eq. (4)

$$\left(\chi(\vec{p})_{\mathrm{lower}}=\frac{\vec{\sigma}\cdot\vec{p}}{E+M}\chi(\vec{p})_{\mathrm{upper}}\right)$$

by $\vec{\sigma}\cdot\vec{p}_{as}$, with $\vec{p}_{as}$ the momentum corresponding to the asymptotic kinematics at the nucleon vertex. Results obtained within this approximation both with relativistic and nonrelativistic potentials were compared to experiment in Ref. [1].

The differences between the calculations of Ref. [18] and those presented in Ref. [1] can be either due to the EMA procedure, or to an additional dynamical relativistic effect different from the Darwin term, namely the enhancement of the lower components (ii): The lower components of the fully relativistic solutions are enhanced at the nuclear interior due to the presence of negative energy components [13,30,40]. Solving the Dirac equation with scalar and vector potentials we see that the lower components are related to the upper ones by

$$\chi(\vec{p})_{\mathrm{lower}}=\frac{\vec{\sigma}\cdot\vec{p}}{E+M+S-V}\chi(\vec{p})_{\mathrm{upper}}. \tag{5}$$

Comparing with Eq. (4), we see that the lower components are enhanced with respect to the ones of free positive energy spinors by a factor

$$A^{-1}(r)=\frac{E+M}{E+M+S(r)-V(r)}$$

(we recall $S<0$, $V>0$, and $A^{-1}(r)$ is $\simeq 2$ at the nuclear interior for the usual values of the potentials). $A^{-1}(r)$ equals the inverse of the Darwin factor squared. This enhancement of the lower components with regard to free spinors has been sometimes referred as *spinor distortion* [29].

As one can see from Eqs. (4) and (5), for small values of the momentum $\vec{p}$ the lower components would play a minor role with respect to the upper ones, due to the factor $\vec{p}/(E+M)$. In this low-p region ($p<300$ MeV), the enhancement of the lower components is not important for the $(e,e'p)$ cross sections [13] and the most visible difference between RDWIA and nonrelativistic (kinematically corrected) DWIA results is caused by the effect mentioned above in point (i), namely, the Darwin term. Due to dynamical effects, relativistic cross sections at low-p are smaller than the nonrelativistic ones and RDWIA-deduced spectroscopic factors from the low-p data are 10 to 15 % higher than the nonrelativistic ones [11,12]. With increasing p, however, the lower components cease to be small and their enhancement, present in the fully relativistic wave functions but not in Eq. (4) or in similar nonrelativistic expressions, increases the cross sections at $p>300$ MeV/c, compared to the nonrelativistic ones. This improves sizeably the agreement with the data of the RDWIA $(e,e'p)$ cross sections [14,15]. In short, in regions where the momenta of the bound and/or final nucleon are comparable to the nucleon mass, the RDWIA cross sections are *larger* than the nonrelativistic DWIA ones, in spite of the Darwin factor that in these kinematical regions would play a minor role. The more visible dynamical effect in high-p regions would be the one mentioned in paragraph (ii) that is, the enhancement of the lower components. This enhancement is crucial to obtain good agreement [15,20] with the recent data for R_{TL} response and A_{TL} in ^{16}O taken at TJNAF for $Q^2\simeq 0.8$ (GeV/c)^2 [20,21].

To compare with nonrelativistic calculations, one can project the negative energy sector out of the fully relativistic solutions, thus removing the enhancement of the lower components described in paragraph (ii). More specifically, if the negative-energy components are projected out, the nucleon current is calculated as

$$J^{\mu}_{\rm proj}(\omega,\vec{q})=\int d\vec{p}\;\overline{\psi}^{(+)}_F(\vec{p}+\vec{q})\hat{J}^{\mu}(\omega,\vec{q})\psi^{(+)}_B(\vec{p}), \qquad (6)$$

where $\psi^{(+)}_B$ ($\psi^{(+)}_F$) is the positive-energy component of ψ_B (ψ_F), i.e., $\psi^{(+)}_B(\vec{p})=\Lambda_{(+)}(\vec{p})\psi_B(\vec{p})$, $\Lambda_{(+)}(\vec{p})=(M+\not{p})/2M$, with $\overline{p}_{\mu}=(\sqrt{\vec{p}^2+M^2},\vec{p}\,)$ (similarly for $\psi^{(+)}_F$). That is, the matrix element of the current is computed in a truncated space with only positive energy spinors without enhancement of the lower components. This truncation is inherent to all nonrelativistic calculations. The dynamical enhancement of the lower components is contained in the current of Eq. (3) but not in Eq. (6). Apart from kinematical effects, the matrix elements obtained with the prescription of Eq. (6) are equivalent to the ones computed in nonrelativistic approaches based upon either the Foldy-Wouthuysen reduction [6,31] or the direct Pauli reduction [13,32].

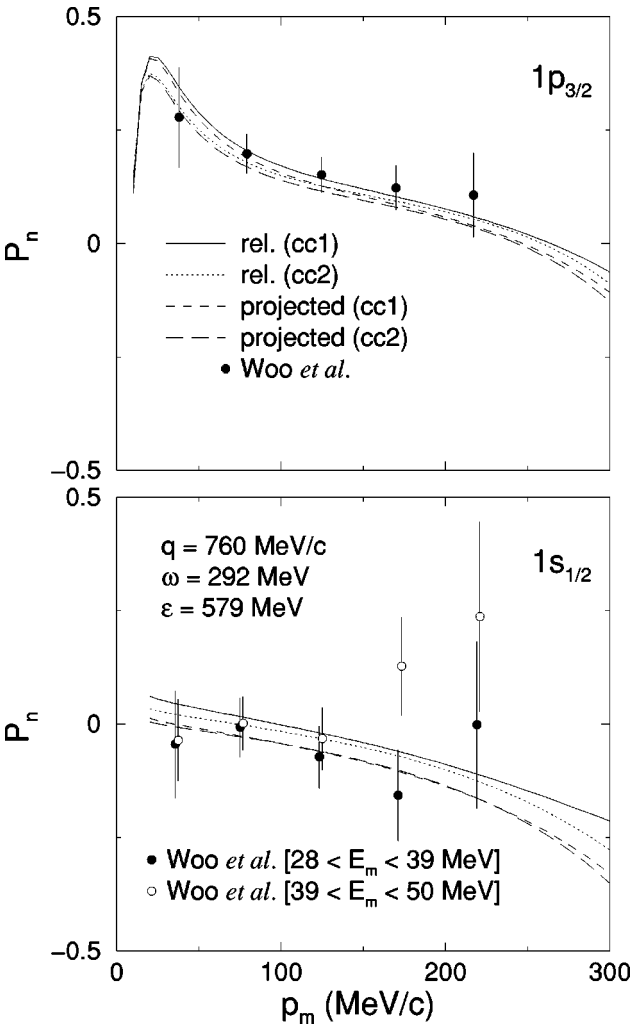

FIG. 1. P_n from ^{12}C for the $1p_{3/2}$ (upper panel) and $1s_{1/2}$ (lower panel) orbits, versus missing momentum p_m in MeV/c. Results shown correspond to a fully relativistic calculation with the $cc1$ (solid) and $cc2$ (dotted) operators. Also shown are the results after projecting the bound and scattered proton wave functions over positive-energy states (short-dashed and long-dashed lines, respectively). Data points are from Ref. [1].

The EMA approach (or more properly the EMA-noSV one where, as we have said, no spinor distortion is considered [29]) also removes the enhancement of the lower components but it is not completely equivalent to the exact projection method. Indeed, it is equivalent to neglecting the p dependence of the projection operators in Eq. (6), using instead the asymptotic values of the momenta at the nucleon vertex. We can say that the EMA-noSV approach computes the matrix element with spinors that have the same structure as the ones that enter in the scattering of free nucleons, because it enforces the relationship between upper and lower

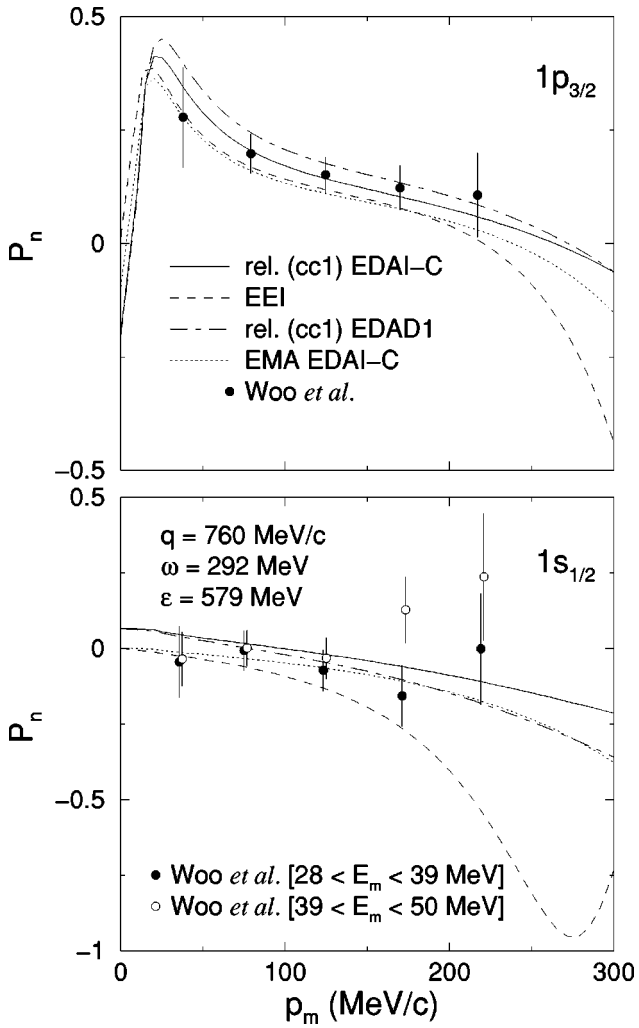

FIG. 2. P_n from ^{12}C for the $1p_{3/2}$ (upper panel) and $1s_{1/2}$ (lower panel) orbits, versus missing momentum p_m in MeV/c. Results shown correspond to a fully relativistic calculation with the $cc1$ and the EDAI-C (solid), and the EDAD1 (dash-dotted) potentials. Also shown are the EMA results (dotted line) for the EDAI-C case. Former EMA-EEI results (dashed line) and data points are from Ref. [1].

components to be driven by the asymptotic value of the momenta at the nucleon vertex. The EMA-noSV calculation lacks any ''spinor distortion,'' exactly as in the scattering of free nucleons. In particular, the Gordon transformation is exact for the EMA-noSV approach and $cc1$ and $cc2$ operators would lead to identical results within EMA-noSV, if the same choices for the off-shell values of ω, E, E', $\vec{P}$, and $\vec{P}'$ are made in both cases.

The projected results, on the other hand, though lacking the large (around a factor of 2) enhancement of the lower components seen in the fully relativistic calculation, are based on spinors whose upper/lower components verify Eq. (4) but with a wider value of momenta than in scattering from free nucleons. Thus, even projected (nonrelativistic) results can have a certain degree of spinor distortion compared to the free case due to the dispersion by the nuclear potentials.

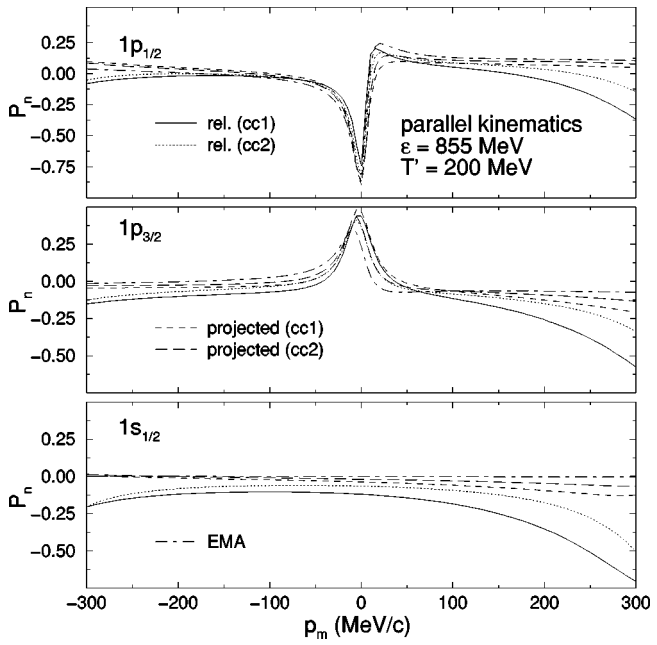

FIG. 3. P_n from ^{16}O for the $1p_{1/2}$ (upper panel), $1p_{3/2}$ (middle panel), and $1s_{1/2}$ (lower panel) orbits, versus missing momentum p_m in MeV/c. Results shown correspond to a fully relativistic calculation with the $cc1$ (solid line) and $cc2$ (dotted line) operators. Also shown are the projected results (short- and long-dashed lines) and the EMA-$cc1$ ones (dash-dotted line). Results in parallel kinematics corresponding to Ref. [3] and the EDAI-O potential is used.

We must keep in mind that both projected and EMA-noSV results still incorporate the dynamical quenching of the upper components (Darwin term) and, if they are to be compared with nonrelativistic calculations, care must be taken of the Darwin term in the nonrelativistic result. Relativistic optical potentials normally give rise to increased absorption and stronger spin-orbit potentials. Due to this, it is expected that they would also lead to a stronger induced normal polarization.

We want to emphasize that the possible differences with the former EMA-noSV analyses of Woo *et al.* [1] are not due to the use of a relativistic optical potential. In both Refs. [1] and [18], results were presented with the same potential EDAI-C that we use in the present work. The Darwin term (leading to increased absorption) was also included in a similar way to us. Thus, if there are differences between our results and those of Ref. [1], they must be due to relativistic effects additional to the Darwin term and different from the fact that the optical potential is relativistic or not.

II. RESULTS

For the bound state wave functions we use the parameters of the set NL3 [33] that reproduces adequately the known momentum distributions at low-p [34]. We have also computed results with other bound state wave functions and found the effects in P_n to be very small up to $p \leqslant 250$ MeV/c. For the scattered proton wave function, we use the energy-dependent A-independent potentials derived by Clark *et al.* for ^{12}C (EDAI-C) and ^{16}O (EDAI-O) [35]. To study

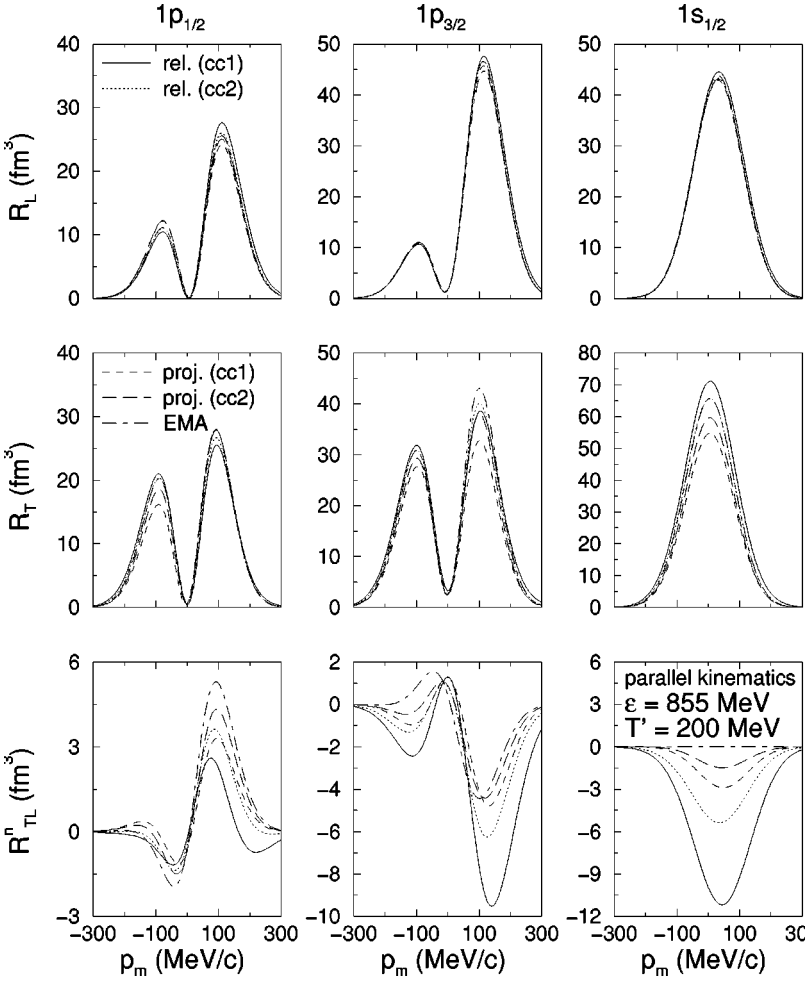

FIG. 4. Response functions corresponding to the kinematics of Fig. 3.

the sensitivity to different optical potentials, we also compute results with the energy-dependent *A*-dependent parametrization 1 (EDAD-1) of Ref. [35].

A. Comparison with former results from Bates

In Fig. 1, P_n is presented against the momentum of the recoiling residual nucleus or *missing momentum* p_m, related to the momentum of the nucleon inside the target nucleus before being knocked out [4]. The results are computed for the kinematics of Ref. [1], namely, beam energy of 580 MeV, kinetic energy of the final nucleon of 270 MeV, $|\vec{q}| \simeq 760$ MeV/c, $\omega \simeq 290$ MeV in q-ω constant kinematics with $Q^2 \simeq 0.5$ (GeV/c)^2. We use the Coulomb gauge in all the cases. We included the Coulomb distortion of the electron wave function and found its effect in P_n to be small. With solid (dotted) lines we present the fully relativistic results obtained with the $cc1$ ($cc2$) operator. We also show results after projecting out the negative energy components (short-dashed lines for $cc1$, long-dashed lines for $cc2$).

We see that for the fully relativistic results, the agreement with the data is excellent in both shells, except perhaps for the highest p_m and missing energy data points in the $s_{1/2}$ shell, where the contribution from continuum states not considered in the present work begins to be important. Looking at the projected results, we see that the removal of the negative energy components worsens the agreement with the data for both the $cc1$ and $cc2$ operators. In all cases P_n is smaller (less positive or more negative) for the projected calculations. We also see that the Gordon ambiguities, i.e., the differences between $cc1$ and $cc2$ results, are rather small. Compared to the theoretical results of Ref. [1], the agreement with experiment is better for any of the curves presented in Fig. 1. This cannot be due only to the negative energy components because the effect of projection is rather modest as the results in Fig. 1 show. To disentangle the reasons for this difference in Fig. 2 we show (dotted lines) a calculation obtained with the EDAI-C potential within the EMA-noSV approach with the operator $cc1$ (very similar results are obtained with the $cc2$ operator and are not shown here). As a guidance, the solid line in Fig. 2 corresponds to the same one of Fig. 1. We see in Fig. 2 that for the EMA-noSV results the reduction of P_n is noticeable and the agreement with the data is worse. Our EMA-noSV results are in the line of the ones obtained with the same optical potential EDAI-C in Ref. [1]. We note that our $cc1$ and $cc2$ results are not identical within EMA-noSV due to the different off-shell prescription we use in each case for the values of the kinematical quantities that enter in the evaluation of the current matrix element. Following Ref. [16] for $cc2$ we have

$$\hat{J}^{\mu}_{cc2} = F_1 \gamma^{\mu} + i \frac{\sigma^{\mu\nu} q_{\nu}}{2M} F_2, \tag{7}$$

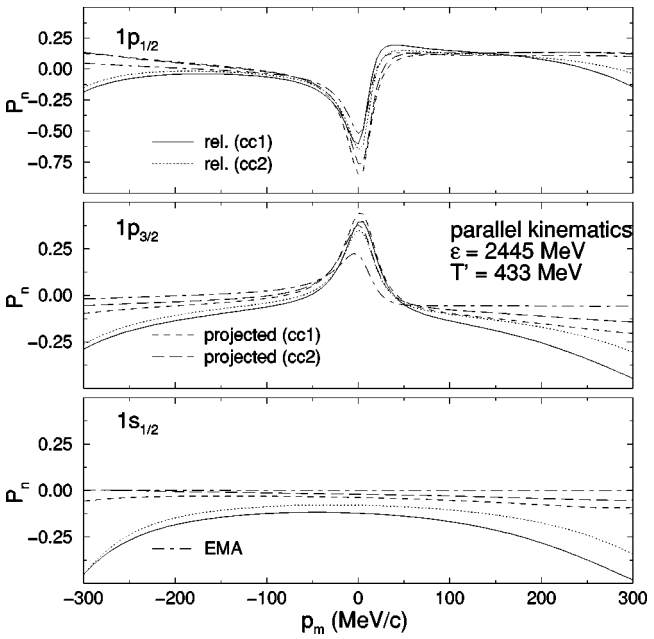

FIG. 5. P_n from ^{16}O for the $1p_{1/2}$ (upper panel), $1p_{3/2}$ (middle panel), and $1s_{1/2}$ (lower panel) orbits, versus missing momentum p_m in MeV/c. Results shown correspond to a fully relativistic calculation with the $cc1$ (solid line) and $cc2$ (dotted line) operators. Also shown are the projected results (short and long dashed lines) and the EMA(noSV)-$cc1$ ones (dash-dotted line). Parallel kinematics suitable at TJNAF [2] and the EDAI-O potential is used.

with $q^\nu=(\omega,\vec{q})$ at the electron vertex. For $cc1$ we have

$$\hat{J}^\mu_{cc1}=(F_1+F_2)\gamma^\mu-\frac{F_2}{2M}(P'+p_m)^\mu, \tag{8}$$

with $p_m=(\overline{E},\vec{p}_m)$, $\vec{p}_m=\vec{P}'-\vec{q}$, $E'=\sqrt{\vec{P}'^2+M^2}$ (the final nucleon is asymptotically on-shell), and $\overline{E}=\sqrt{\vec{p}_m{}^2+M^2}$. Thus, ω used in Eq. (7) is different from $\overline{\omega}=E'-\overline{E}$ as implied in Eq. (8). If we had used $\overline{\omega}$ in $cc2$ instead of ω, the results of our $cc1$ and $cc2$ EMA-noSV calculations would be identical. At present, there is no definite prescription for handling this off-shell kinematical ambiguity in ω, $\overline{\omega}$ and other kinematical variables to be used in the current operator [23,24]. This ambiguity arises because, contrary to the scattering of free nucleons, part of the energy and momentum of the exchanged photon is transferred to the recoiling system instead of being completely absorbed by the detected nucleon. We have chosen the original prescription of de Forest of using $\overline{E}$ in $cc1$ but ω in $cc2$. We find that, in this way, off-shell kinematics ambiguity effects and Gordon ambiguity ones reinforce each other so that the differences between the $cc1$ and $cc2$ results are enhanced by our choice. The EMA-noSV results are free from Gordon ambiguities. This is the reason why $cc1$ and $cc2$ results obtained in such approach are much closer than the corresponding ones of the full RDWIA calculations. Kinematical ambiguities will cause differences of up to 15% between our $cc1$ and $cc2$ EMA-noSV unpolarized cross-section results for all the cases considered in the present work. However, the effect of these ambiguities in the P_n predictions is almost negligible (typically less than 1%). We have plotted only the $cc1$ EMA-noSV result for P_n. Our $cc2$ EMA-noSV result is almost identical to this curve.

TABLE I. Approximated values of the kinematical variables and the factors in Eq. (2) for the q-ω constant experimental setups discussed in the present work.

	TJNAF	MAMI	Bates
θ_e	23.4°	48.8°	118.8°
Q^2 (GeV/c)^2	0.8	0.4	0.5
ω (MeV)	445	215	292
V_L	0.643	0.792	0.727
V_T	0.444	0.651	3.283
V_{TL}	0.737	0.932	1.642
V_{TT}	0.401	0.445	0.426

Recently, Kelly has incorporated the effect of spinor distortion within his EMA approach by including the relativistic potentials in the lower component of the spinors as in Eq. (5), while still substituting the $\vec{\sigma}\cdot\vec{p}$ term by $\vec{\sigma}\cdot\vec{p}_{\rm as}$. This is called EMA-SV approach in Ref. [29] in contrast to EMA-noSV. This procedure reintroduces the dynamical enhancement of the lower components. For modest values of the momentum (up to around 275 MeV/c), where the role of the lower components is less relevant, this approximation goes close [39] to the results obtained with the exact treatment that we do in the present work. It tends, however, to minimize the effect of enhancement of the lower components beyond the value of p_m mentioned above and, as the momentum of the ejected nucleon is normally well above 275 MeV/c, it underestimates the effect of spinor distortion for the ejected nucleon. We conclude that an important reason for the differences of our full RDWIA results with those of Ref. [1], using the same optical potential EDAI-C, is the EMA-noSV approach employed in Ref. [1].

For the purpose of comparison, we present (dash-dotted line in Fig. 2) results obtained with the same bound state wave functions as for the other curves, the full RDWIA approach with the $cc1$ operator but a different optical potential, namely, the EDAD-1 of Ref. [35]. We emphasize that the EDAI-C potential should be a more suitable choice than EDAD-1 for ^{12}C because it describes better the elastic proton scattering data for this particular nucleus. The effect of using EDAD-1 instead of EDAI-C is sizable. EDAD-1 yields a larger P_n for the $p_{3/2}$ shell, worsening the agreement with the data and a smaller P_n for the $s_{1/2}$ shell, with no significant worse (or better) agreement with the data in this shell. We observed that both EDAI-C and EDAD-1 produce almost identical unpolarized cross sections or unpolarized response. However, the P_n values they produce are noticeably different. This shows the sensitivity of P_n to details of the FSI.

The comparison between the results of both potentials follows the same general trend as shown in Ref. [18]. In Ref.

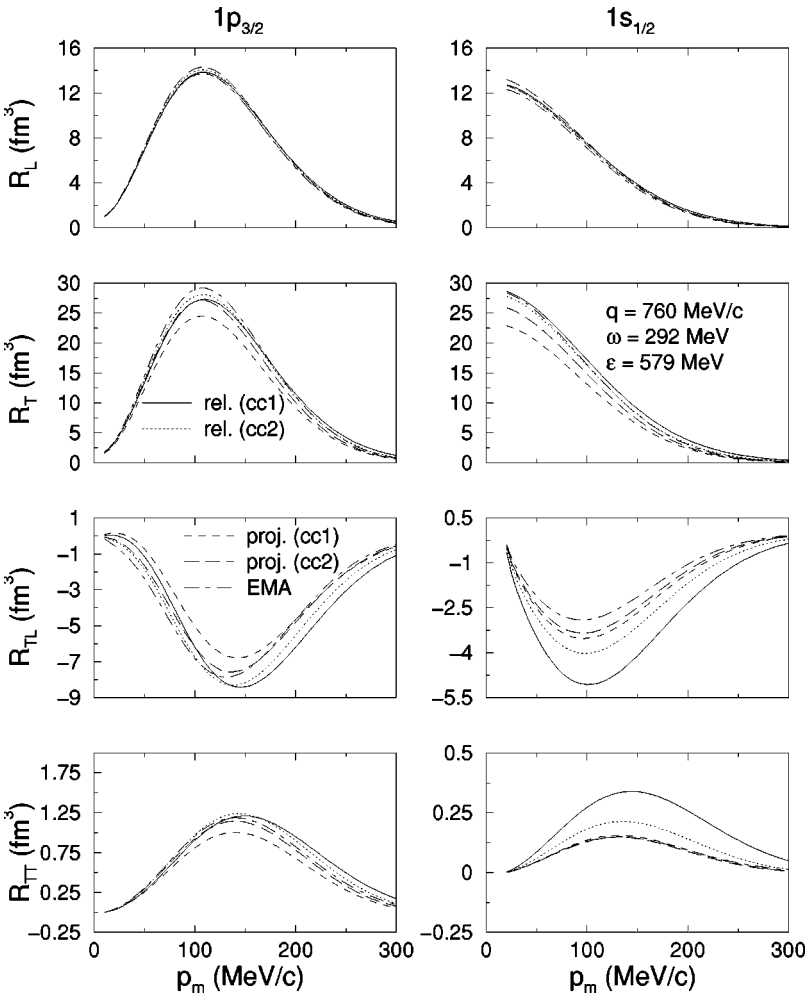

FIG. 6. Unpolarized responses for the kinematics of Fig. 1.

[18], P_n changes in the same relative direction in going from EDAI-C to EDAD-1 as in our calculation but, contrary to our case, the differences between the EDAI-C and EDAD-1 are larger for the $1s_{1/2}$ shell than for the $1p_{3/2}$ one and in this latter shell, their results seem to agree better with experiment for the EDAD-1 potential than for the EDAI-C. We find, in general, that our results with EDAI-C agree better with the data. These minor discrepancies with Ref. [18] should be traced back to the different bound state wave functions and possibly other parts of the formalism (current operator, Coulomb distortion) employed in both cases.

In Fig. 2 we also show the EMA-noSV results of Ref. [1] with the EEI potential (dashed line). In Ref. [1] a more positive P_n for the $p_{3/2}$ shell and better agreement with the data was obtained with the EEI potential than with the EDAI-C one. For the $1s_{1/2}$ shell, however, a more negative P_n and worse agreement with the data was found.

The EMA-noSV-EEI calculation of Ref. [1] underestimated the data by about 10%. The EEI is a nonrelativistic optical potential obtained after folding a density dependent empirical effective interaction with the nuclear density [37]. The interaction is fitted to proton-nucleus elastic *and inelastic* scattering data for several states of several targets simultaneously. The relativistic optical potentials, on the other hand, are fitted only to elastic scattering data. It is well known that elastic data can only constrain the asymptotic part of the potentials. Given the fact that the nucleus is almost transparent to electrons (compared to nucleons), phase-shift equivalent potentials that differ only in the nuclear interior would produce the same good fits to elastic proton scattering observables, leading, however, to different electron scattering results. The EEI approach solves this ambiguity by phenomenologically constraining the potentials in the nuclear interior by means of simultaneous fits to inelastic data. In the relativistic case, on the other hand, the shape of the potentials at the nuclear interior is assumed to be of simple Woods-Saxon+surface terms, not very different from what one finds in the relativistic mean field approximation. Thus, the fact that the relativistic model gives a very fair account of $(e,e'\vec{p})$ observables such as P_n cannot be attributed merely to the incorporation of the right phenomenology, as it could be the case with the EEI potentials, but to a merit of the model itself.

B. Predictions for Mainz and TJNAF in parallel kinematics

In a recent work [15,20,38], it has been shown that the dynamical enhancement of the lower components shows up differently in the $j=l-1/2$ and $j=l+1/2$ spin-orbit partners, specially for the R_{TL} response and the A_{TL} asymmetry. We remind that for ^{12}C the two shells studied correspond to $j=l+1/2$ spin-orbit partners. New sets of induced polariza-

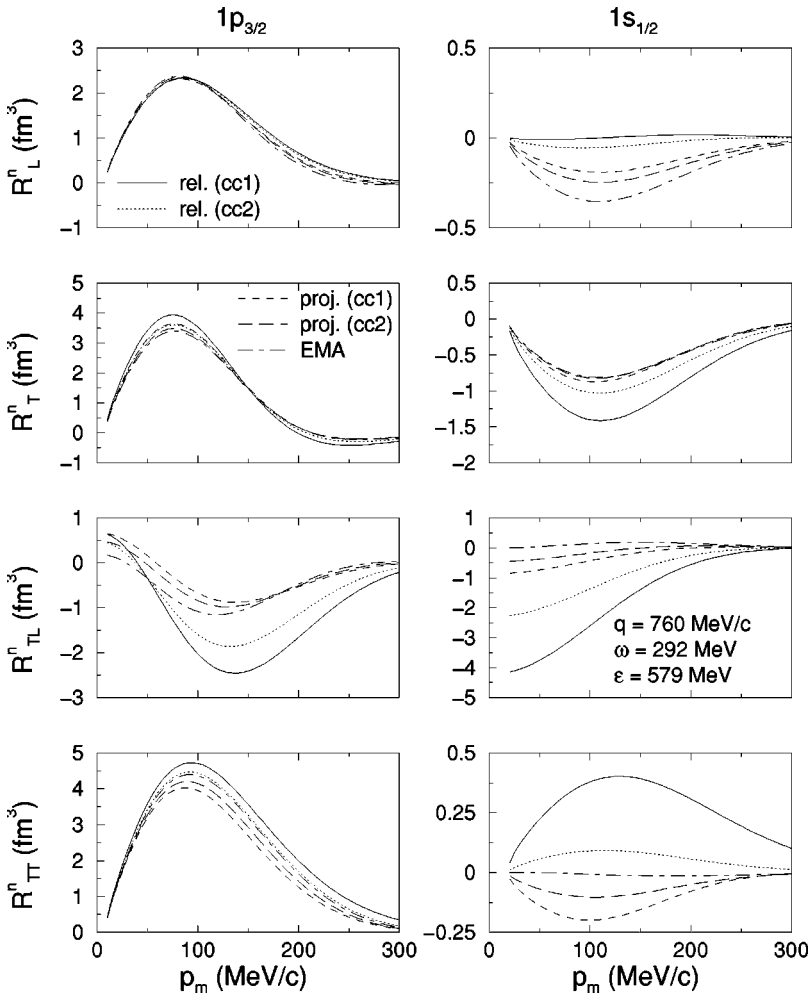

FIG. 7. Normal responses for the kinematics of Fig. 1.

tion P_n are being obtained at TJNAF [2] in ^{16}O at a more relativistic kinematics, namely, beam energy of 2450 MeV, kinetic energy of the ejected nucleon of about 420 MeV, and $Q^2 \simeq 0.8$ (GeV/c)^2. There is also a proposal at Mainz [3] to do similar measurements at a smaller value of the kinetic energy of the ejected nucleon, namely 200 MeV. In what follows, we analyze whether these experiments may provide signatures of relativistic dynamics in P_n similar to the ones found in R_{TL} and A_{TL}.

In parallel kinematics only two responses, R_L and R_T, contribute to the unpolarized cross section and just one, R^n_{TL}, to P_n, so that for this kinematics the analyses are simplified. We present in Fig. 3 fully RDWIA results with $cc1$ (solid line), $cc2$ (dotted line), projected results (short-dashed lines for $cc1$ and long-dashed lines for $cc2$), and EMA-noSV results with the $cc1$ operator (dash-dotted line) for the two p-shell spin-orbit partners of ^{16}O, plus the deep s shell, in parallel kinematics and with beam energy and transfer energy suitable for Mainz [3] (beam energy of 855 MeV, kinetic energy of the ejected nucleon of 200 MeV).

For the three shells we see the opposite pattern to the one depicted in Fig. 1: the removal of the negative energy components drives here P_n towards higher values, and even more so does using the EMA-noSV approach. For the kinematics of Fig. 3, the effect of projection and Gordon ambiguities is much larger than it was in Fig. 1.

A very characteristic feature is seen in the $s_{1/2}$ shell for this case of parallel kinematics: A zero value of P_n is predicted within the EMA-noSV approach. A small value of P_n is obtained by the projected calculations, while the full RDWIA approach yields a relatively large (in absolute value) P_n due to spinor distortions. The choice $cc1$, that emphasizes the effect of the enhancement of the lower components [30], yields the largest prediction for P_n in absolute value. Should the experiments at TJNAF or Mainz provide us with P_n values with equal or smaller uncertainty that the ones already measured at Bates, it will undoubtedly disentangle the role played in P_n by the enhancement of the lower components.

The responses involved in the evaluation of P_n for this case are displayed in Fig. 4. The only nonzero contribution to P_n comes from R^n_{TL} and the link between the responses shown in the bottom panel of Fig. 4 and the results for P_n of Fig. 3 is straightforward. As it could be deduced from the values of P_n displayed in Fig. 3, R^n_{TL} for the $s_{1/2}$ shell is zero within EMA-noSV, it is very small for the projected results and reaches the largest absolute value for the full RDWIA $cc1$ calculation. The results for the $p_{3/2}$ shell follow the same trend as shown for the $s_{1/2}$ shell, only that here the more complex spin-orbit structure of the bound state causes a nonzero value of P_n even for the EMA-noSV results. The pro-

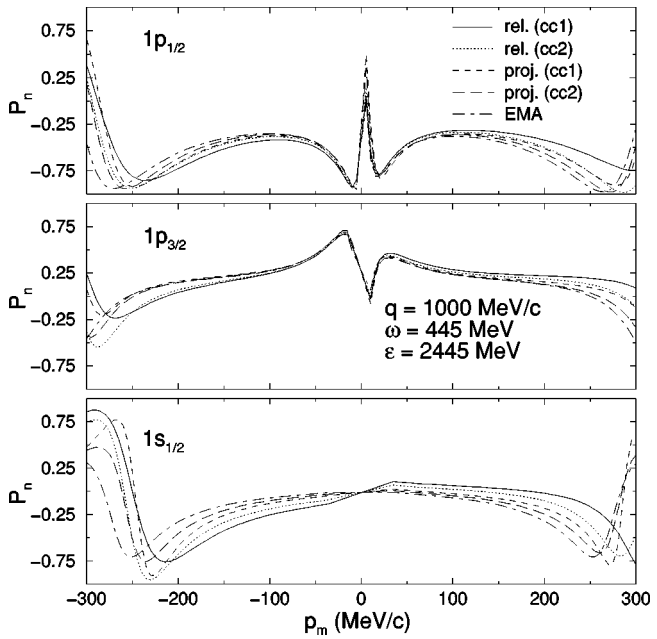

FIG. 8. P_n from ^{16}O for the $1p_{1/2}$ (upper panel), $1p_{3/2}$ (middle panel), and $1s_{1/2}$ (lower panel) orbits, versus missing momentum p_m in MeV/c. Results shown correspond to a fully relativistic calculation with the $cc1$ (solid line) and $cc2$ (dotted line) operators. Also shown are the projected results (short and long dashed lines) and the EMA(noSV)-$cc1$ ones (dash-dotted line). Results in q-ω constant kinematics corresponding to Ref. [2] and the EDAI-O potential is used.

jected and EMA-noSV results display small (in absolute value) predictions for R_{TL}^n. The $cc2$ RDWIA prediction exhibits larger R_{TL}^n, while the full $cc1$ result yields the largest value of R_{TL}^n. This gradation of R_{TL}^n is similar to what one finds generally for the unpolarized R_{TL} (in q-ω constant kinematics): As the $cc1$ operator enhances the role of the negative energy components [30] with regards to other choices of the operator, it produces the largest value of R_{TL}. Thus, at least for the $j=l+1/2$ spin orbit partner, we observe the same behavior for R_{TL}^n and R_{TL} with regards to the effect of negative energy components.

On the other hand, we find that projection and Gordon ambiguities effects show up differently for the $p_{1/2}$ shell. For this case R_L, R_T, and R_{TL}^n are shown in the leftermost panel of Fig. 4 at the same kinematics of Fig. 3. While for R_{TL}^n in the $j=l+1/2$ shells the larger was the role given to the negative energy components the larger (in absolute value) R_{TL}^n response was obtained, for the $p_{1/2}$ shell ($j=l-1/2$) one sees the opposite behavior: the full $cc1$ calculation yields the smallest R_{TL}^n while the EMA-noSV prediction displays the largest one. This is at variance with the behavior observed for the unpolarized R_{TL} response [38] and indicates an interference between positive and negative energy component contributions to R_{TL}^n. This interference is constructive for the $j=l+1/2$ shells so that the calculations with large contribution from negative energy components yield a large R_{TL}^n, while it is largely destructive for the $j=l-1/2$ shells for which large effects of negative energy components translate into small values of R_{TL}^n.

In Ref. [36] results were presented for the EMA-noSV case within the IA and also in a calculation beyond IA that included channel coupling to several configurations in the final state. Our EMA-noSV result of Fig. 4 and the one shown in Fig. 14 of Ref. [36] are very similar, with small differences due to the different wave functions and optical potentials. The most interesting outcome of this comparison is that the effect of spinor distortion increases R_{TL}^n, in particular for the case of the $s_{1/2}$ shell that would have a zero value without spinor distortion within IA. Due to channel coupling (CC), a nonzero R_{TL}^n for this shell was obtained in Ref. [36]. The effect of spinor distortion, however, is at least twice to four times (depending on whether one considers the RDWIA $cc2$ or $cc1$ result) larger than the one of CC shown in Ref. [36]. We conclude that coupled channel contributions would not mask the large negative value of P_n caused by spinor distortion. The R_{TL}^n response in this $s_{1/2}$ shell is sensitive to Gordon ambiguities and overall constitutes a very clear signature for the presence of negative energy components in the nucleon wave function.

For the other shells, the effects of CC shown in Ref. [36] were small at moderate values of p_m for the cases we studied in the present work and the IA results shown here should not change much if CC effects were considered. Still in parallel kinematics but with a larger value of Q^2 that is suitable at TJNAF, we have obtained very similar results to the ones just presented. We plot in Fig. 5 only the results for P_n.

C. q-ω constant kinematics

The experiment of Bates was performed in q-ω constant kinematics and in the same side of $\vec{q}$ for the scattered proton, $\phi'=\pi$, which corresponds to $p_m>0$ in our figures. The analysis of this case is more complicated because all the eight responses of Eq. (2), in combination with the factors shown in Table I, contribute to the cross section and P_n. In Figs. 6 and 7 we present the responses for the Bates results depicted in Fig. 1. The effect of spinor distortion and Gordon ambiguities in the R_L, R_T, R_{TL}, and R_{TT} has been studied previously in the context of RPWIA [30,38]. It was found there that for the $j=l+1/2$ partners, as it is the case of the two shells in ^{12}C, the differences are relatively small, at least for the ''large'' responses R_L and R_T.

For the normal responses the situation is less clear. One must remember that unpolarized and normal responses share the same structure in terms of components of the hadronic current, differing only in the signs with which the contribution for every value of ejected nucleon spin projection upon the normal direction enters into the unpolarized or normal responses [5,7]. Thus, large unpolarized responses usually come from constructive interference of the two spin contributions and are associated with a correspondingly small normal response coming from destructive interference. The converse is also true: small unpolarized responses have a correspondingly large polarized normal response [7]. If there were no FSI, both normal projection contributions (spin up and spin down) would be identical, all the responses shown

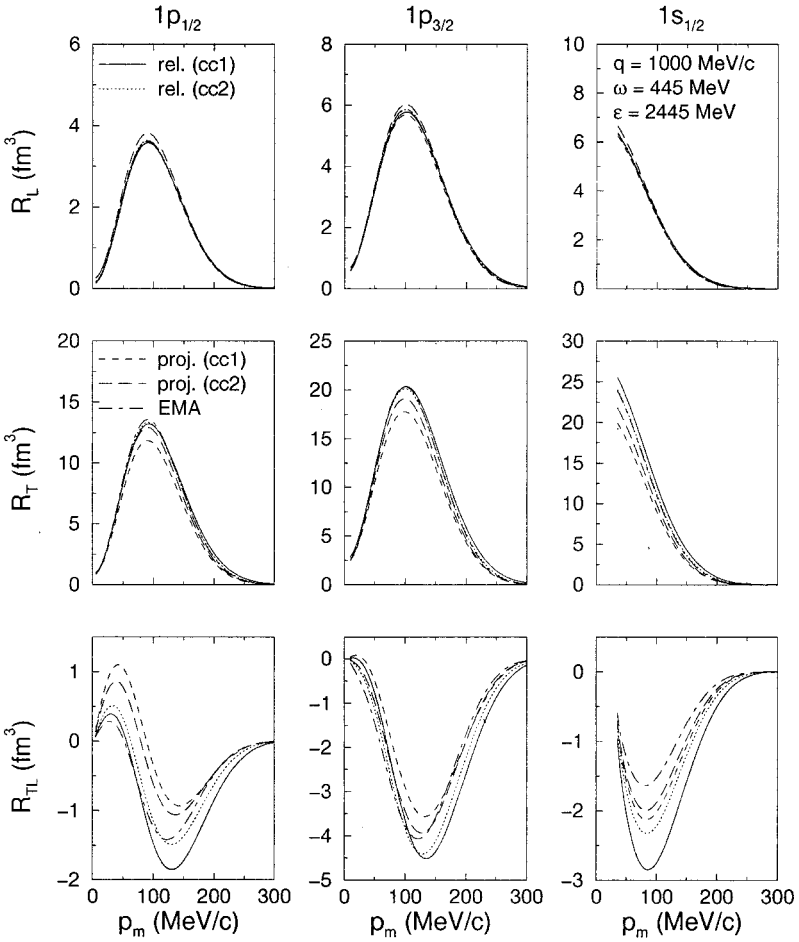

FIG. 9. Unpolarized responses for the kinematics of Fig. 8. The response R_{TT} is not plotted, because it is much smaller than the ones shown.

in Fig. 7 would vanish and no normal polarization would be observed.

Taking into account the value of the kinematical factors in front of each response (see Table I), the main contributions to P_n for the $s_{1/2}$ shell comes from R_T^n and R_{TL}^n responses. In the case of the full RDWIA results, the R_{TL}^n response is responsible for most of the net P_n. Due to this, P_n will change sign with p_m because of the cos ϕ' factor in Eq. (2). We also see that R_{TL}^n is larger (in absolute value) for the calculation with larger effect of the negative energy components, i.e., the full $cc1$ result. In Fig. 6 we can see the same feature in the unpolarized R_{TL} response. This characteristic has been explained before [20,30,38]. For the p shell, the largest contribution comes from R_T^n that shows little dependence on spinor distortion. This is why the effect of negative energy components is small for this shell.

We plot also P_n and responses (Figs. 8, 9, and 10) for a kinematics suitable at TJNAF (namely $|\vec{q}|=1000$ MeV/c, $\omega=445$ MeV and energy of the beam $\epsilon=2445$ MeV). Apart from what has been already said, we find that for the $p_{3/2}$ shell and $p_m<0$ there are small Gordon ambiguities and a very clear separation of the fully RDWIA results from the projected or EMA-noSV ones is seen. Therefore, this is a good region to look for the effects of spinor distortion. We can explain this better by looking at the results in the second column of Fig. 10. There, all calculations lie very close except for R_{TL}^n. In the $p_{3/2}$ shell the projected and EMA-noSV curves group together, while both fully relativistic calculations clearly deviate from the others. Going back to P_n in the second panel of Fig. 8, we observe these differences only in the region $p_m<0$, due to the different sign with which the $\cos\phi' R_{TL}^n$ term contributes in the $p_m<0$ and $p_m>0$ regions. This behavior is characteristic of the kinematics chosen at TJNAF. Indeed, as we can see in Fig. 11, at different kinematics conditions such as the ones suitable at Mainz (i.e., q-ω constant kinematics with $|\vec{q}|=648$ MeV/c, $\omega=215$ MeV, and $\epsilon=855$ MeV), there is not such a clear separation of the fully relativistic curves from the others in the $p_{3/2}$ shell for $p_m<0$ as the one found for the TJNAF kinematics. Another interesting feature that was already found in parallel kinematics is that, for the $j=l+1/2$ shells, R_{TL}^n has larger values when the calculation emphasizes the role of negative energy components while the converse is seen for the $p_{1/2}$ ($j=l-1/2$) shell.

For the two p shells at the kinematics of TJNAF and Mainz, the largest contribution to P_n would come from $V_{TT}R_{TT}^n$. For the $p_{3/2}$ shell in the $p_m<0$ region, however, this contribution is canceled to a large extent by the $V_{TL}R_{TL}^n$ one. This explains why P_n is mainly negative for $p_m<0$ for the $p_{3/2}$ shell. On the other hand, the $v_{TL}R_{TL}^n$ contribution is less important for the $p_{1/2}$ shell and practically does not influence the total polarization. Therefore P_n for this shell is negative irrespectively of the sign of p_m.

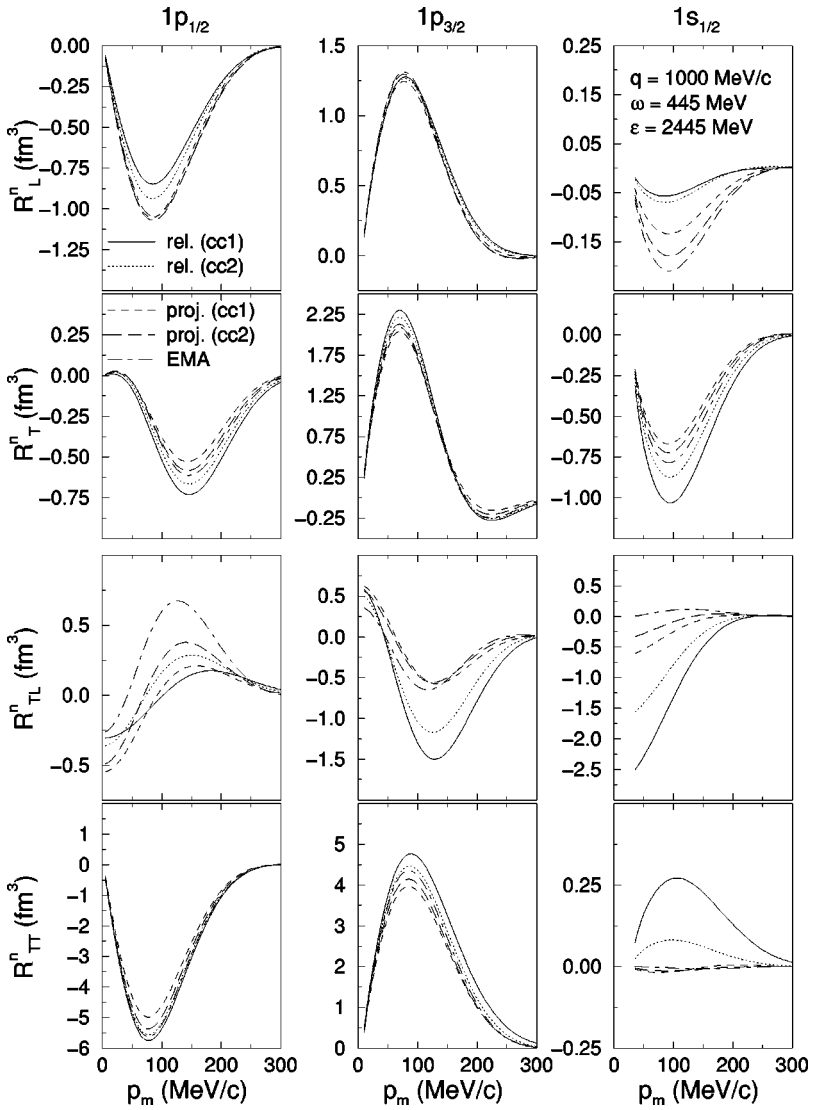

FIG. 10. Normal responses for the kinematics of Fig. 8.

A serious concern is the issue of current conservation. The use of an optical potential breaks gauge invariance in DWIA. We estimated the uncertainty associated to the choice of gauge by comparing the results we show in the present work with the ones obtained in the Landau gauge. We find that the fully relativistic results in perpendicular kinematics at the highest value of Q^2 are the less sensitive ones to this procedure. On the other hand, the unpolarized cross sections can differ by as much as 50% in parallel kinematics for large values of $|p_m|$. However, P_n is much less sensitive to the choice of gauge than unpolarized cross sections: For the fully RDWIA results of the present work, using the Landau or Coulomb Gauge produces P_n results within 5%. Gauge ambiguity is much less important than the one due to the $cc1$ or $cc2$ choice.

III. CONCLUSIONS

We have found that the relativistic dynamical effect mentioned in paragraph (ii), the enhancement of the lower components, increases noticeably P_n with respect to both the projected and, more sizeably, the EMA-noSV results, driving the fully RDWIA results for P_n into excellent agreement with the data of Ref. [1]. For the kinematics of the TJNAF 89-033 [2] and Mainz [3] experiments we find the differences between the RDWIA and projected results to be important.

P_n proves to be very sensitive to the choice of optical potential, allowing this observable to be used to constrain the theoretical model for FSI so that these effects can be included with confidence when making predictions for other observables much less sensitive to the choice of FSI, such as the polarization transfer observables P'_x and P'_z [29].

Previous explorations of the role of meson exchange currents (MEC) for Bates, based upon a nonrelativistic picture, showed very little effect in P_n at moderate p_m [8]. MEC are expected to play an even minor role for higher Q^2 at quasielastic kinematics ($x \simeq 1$) [8] and its inclusion will not modify substantially the predictions for P_n presented in the present work. The same can be said of coupled channel effects analyzed within the EMA-noSV approach in Ref. [36]. However, Gordon and kinematical off-shellness ambiguities are large for high Q^2 experiments. We have

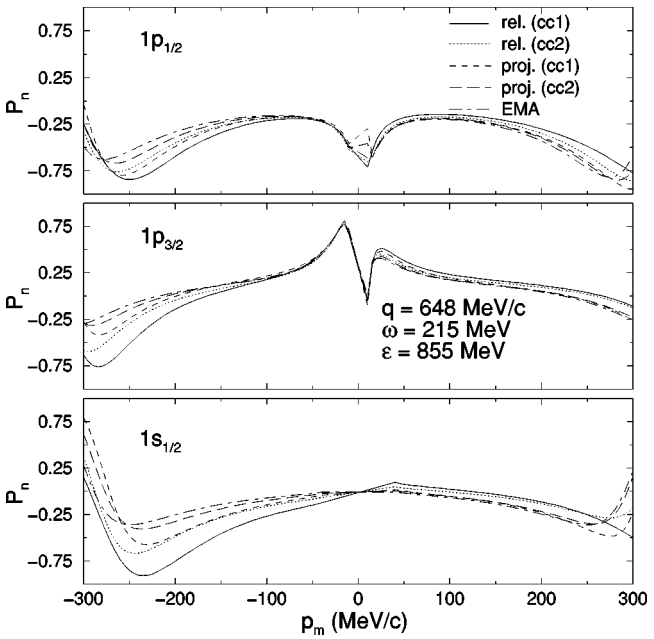

FIG. 11. The same as Fig. 8 except for slightly smaller values of q and P' as expected at Mainz [3].

looked for kinematical regions where these ambiguities are minimized. In parallel kinematics, we conclude that the $p_m<0$ region ($|\vec{q}|>|\vec{P'}|$) is optimal because it displays a minimum effect of Gordon ambiguities while a high sensitivity of the calculations to the presence of negative energy components is found. In q-ω constant kinematics the same favorable situation is seen again for $p_m<0$ ($\phi'=0$) but only for the $p_{3/2}$ shell at $|\vec{q}|=1$ GeV/c, adequate to TJNAF.

In parallel kinematics we found very clear signatures for negative energy components in the wave functions, that cause P_n to be driven towards more negative values with respect to the nonrelativistic prediction, particularly for the $s_{1/2}$ and $p_{3/2}$ ($j=l+1/2$) shells. This feature should remain even in the presence of MEC and CC.

In q-ω constant kinematics the effect of the negative components is manifested as an increase (decrease) of P_n for $p_m>0$ ($p_m<0$) of the relativistic predictions with regards to the nonrelativistic ones. Finally, we hope that future experiments will shed light on the theoretical uncertainties that are still present in the calculations such as which current operator should be used and will help to disentangle the role played by the negative energy components of the wave functions.

ACKNOWLEDGMENTS

This work was partially supported under Contracts No. PB/96-0604 (DGES, Spain) and PR156/97 (Complutense University, Spain). J.M.U. thanks E. Moya de Guerra and J. A. Caballero for many useful comments. We also thank J. J. Kelly for providing us with files with his calculations and interesting comments. J.R.V. acknowledges financial support from the Consejería de Educación y Cultura de la Comunidad de Madrid.

[1] R.J. Woo *et al.*, Phys. Rev. Lett. **80**, 456 (1998).
[2] TJNAF proposal 89-033 (unpublished), C. Glashausser contact person.
[3] R. Neuhasen *et al.*, MAMI Proposal No. A1/2-93, 1993 (unpublished).
[4] S. Boffi, C. Giusti, and F.D. Pacati, Phys. Rep. **226**, 1 (1993); S. Boffi, C. Giusti, F. Pacati, and M. Radici, *Electromagnetic Response of Atomic Nuclei* (Clarendon, Oxford, 1996); J.J. Kelly, Adv. Nucl. Phys. **23**, 77 (1996).
[5] A.S. Raskin and T.W. Donnelly, Ann. Phys. (N.Y.) **191**, 78 (1989).
[6] C. Giusti and F.D. Pacati, Nucl. Phys. **A504**, 685 (1989).
[7] A. Picklesimer and J.W. Van Orden, Phys. Rev. C **35**, 266 (1987); **40**, 290 (1989).
[8] J. Ryckebusch, D. Debruyne, W.V. Nespen, and S. Janssen, Phys. Rev. C **60**, 034604 (1999).
[9] L. Lapikás, G. van der Steenhoven, L. Frankfurt, M. Strikman, and M. Zhalov, Phys. Rev. C **61**, 064325 (2000).
[10] G. Jacob, T.A.J. Maris, C. Schneider, and M.R. Teodoro, Nucl. Phys. **A257**, 517 (1976).
[11] J.P. McDermott, Phys. Rev. Lett. **65**, 1991 (1990); Y. Jin, D.S. Onley, and L.E. Wright, Phys. Rev. C **45**, 1311 (1992).
[12] J.M. Udías, P. Sarriguren, E. Moya de Guerra, E. Garrido, and J.A. Caballero, Phys. Rev. C **48**, 2731 (1993).
[13] J.M. Udías, P. Sarriguren, E. Moya de Guerra, E. Garrido, and J.A. Caballero, Phys. Rev. C **51**, 3246 (1995).
[14] J.M. Udías, P. Sarriguren, E. Moya de Guerra, and J.A. Caballero, Phys. Rev. C **53**, R1488 (1996).
[15] J.M. Udías *et al.*, in *Proceedings of the 4th Workshop on Electromagnetically Induced Two-Hadron Emission*, Granada, 1999, edited by C. Garcia Recio, P. Grabmayr, A. M. Lallena, and R. Owens, ISBN 84-699-1645-9, p. 318.
[16] T. de Forest, Nucl. Phys. **A392**, 232 (1983).
[17] B.D. Serot and J.D. Walecka, Adv. Nucl. Phys. **16**, 1 (1986).
[18] J.J. Johansson and H.S. Sherif, Phys. Rev. C **59**, 3481 (1999).
[19] J.E. Amaro *et al.*, Nucl. Phys. **A602**, 263 (1996).
[20] J.M. Udías *et al.*, Phys. Rev. Lett. **83**, 5451 (1999).
[21] J. Gao *et al.*, Phys. Rev. Lett. **98**, 3265 (2000).
[22] S. Boffi, C. Giusti, F.D. Pacati, and F. Cannata, Nuovo Cimento **98**, 291 (1987).
[23] S.J. Pollock, H.W.L. Naus, and J.H. Koch, Phys. Rev. C **53**, 2304 (1996).
[24] S. Jeschonnek and T.W. Donnelly, Phys. Rev. C **57**, 2438 (1998); J.A. Caballero, T.W. Donnelly, and G.I. Poulis, Nucl. Phys. **A555**, 709 (1993).
[25] G.H. Rawitscher, Phys. Rev. C **31**, 1173 (1985).
[26] J.J. Kelly, Phys. Rev. C **54**, 2547 (1996).
[27] Y. Jin and D.S. Onley, Phys. Rev. C **50**, 377 (1994).
[28] C.G. Darwin, Proc. R. Soc. London, Ser. A **118**, 654 (1928).
[29] J.J. Kelly, Phys. Rev. C **56**, 2672 (1997); **60**, 044609 (1999).

[30] J.A. Caballero, T.W. Donnelly, E. Moya de Guerra, and J.M. Udías, Nucl. Phys. **A632**, 323 (1998).
[31] K.V. McVoy and L. van Hove, Phys. Rev. **125**, 1034 (1962).
[32] H.W. Fearing, G. Poulis, and S. Scherer, Nucl. Phys. **A570**, 657 (1994).
[33] G.A. Lalazissis, J. König, and P. Ring, Phys. Rev. C **55**, 540 (1997).
[34] G. van der Steenhoven *et al.*, Nucl. Phys. **A480**, 547 (1988).
[35] E.D. Cooper, S. Hama, B.C. Clark, and R.L. Mercer, Phys. Rev. C **47**, 297 (1993).
[36] J.J. Kelly, Phys. Rev. C **59**, 3256 (1999).
[37] J.J. Kelly, Phys. Rev. C **39**, 2120 (1989).
[38] J.A. Caballero, T.W. Donnelly, E. Moya de Guerra, and J.M. Udías, Nucl. Phys. **A643**, 189 (1998).
[39] J.J. Kelly (private communication).
[40] S. Ulrych and H. Müther, Nucl. Phys. **A641**, 499 (1998).